Nanocomposites of 2D-MoS$_2$ Exfoliated in Thermotropic Liquid Crystals

Uri R. Gabinet, Changyeon Lee, Ryan Poling-Skutvik, Daniel Keane, Na Kyung Kim, Ruiqi Dong, Zachariah Vicars, Yusheng Cai, Aniket U. Thosar, Alexander Grun, Sarah M. Thompson, Amish J. Patel, Cherie R. Kagan, Russell J. Composto, and Chinedum O. Osuji*

Read Online

ACCESS | Metrics & More | Article Recommendations | Supporting Information

ABSTRACT: Atomically thin MoS$_2$ nanosheets are of interest due to unique electronic, optical, and catalytic properties that are absent in the bulk material. Methods to prepare nanosheets from bulk material that facilitate studies of 2D-MoS$_2$ and the fabrication of useful devices have consequently assumed considerable importance. Here, we report the simultaneous exfoliation and stable dispersion of MoS$_2$ nanosheets in a liquid crystal. Exfoliation of bulk MoS$_2$ in mesogen-containing solutions produced stable dispersions of 2D-MoS$_2$ that retained suspension stability for several weeks. Solvent removal in cast films yielded nanocomposites of 2D-MoS$_2$. Preservation of single- and few-sheet MoS$_2$ was confirmed utilizing UV−vis and Raman spectroscopy in the nematic and isotropic fluid states of the system and, remarkably, in the solid crystal as well. Importantly, the MoS$_2$ nanosheets remained well-dispersed upon polymerization of the reactive mesogen to form a liquid crystal polymer. The ability to stably disperse 2D-MoS$_2$ in a structured fluid opens up new possibilities for studying anisotropic properties of MoS$_2$ and for exploiting such properties in responsive materials.
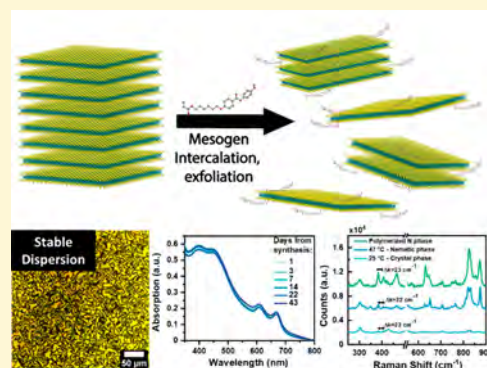
Atomically thin 2D nanomaterials are of considerable interest due to unique properties not present in the bulk materials.[1−8] Transition metal dichalcogenides (TMDs), and specifically MoS$_2$, have attracted significant attention due to their remarkable electronic, optical, mechanical, and catalytic properties.[3,5,9,10] 2D MoS$_2$ is composed of three atomic layers, with a layer of molybdenum sandwiched between two sulfur layers. This structure leads to strong in-plane covalent bonds within the sheets, whereas multiple sheets are held together by weak Van der Waals interactions, with a characteristic spacing of ∼6.5 Å in between sheets.[3] 2D-MoS$_2$ can occur in the hexagonal semiconducting (2H) phase or as the octahedral metallic (1T) phase.[11] Semiconducting (2H) MoS$_2$ exhibits a direct band gap of 1.9 eV,[12] strong photoluminescence,[13] and, as recently reported, a nonlinear optical response.[14−16] Metallic (1T) MoS$_2$, most commonly synthesized by exfoliation following Li intercalation,[17] is especially suitable for energy applications such as batteries[18] and supercapacitors[19] or in catalysis.[20,21] Due to the anisotropic nature of 2D MoS$_2$ sheets, some of the aforementioned properties or application performance of (2H) or (1T) MoS$_2$ can vary significantly depending on the orientation of the sheets. Enhanced catalytic activity of (1T) MoS$_2$ has been identified on vertically oriented sheets,[22,23] owing to the higher exposure of edge sites. Vertical orientation

can also be beneficial in transport- or intercalation-oriented applications, such as membranes[24] or energy storage,[25] where ion diffusion through the sheets can benefit from a direct transport route. The optical response of MoS$_2$ can also be modulated according to the sheets' orientation,[26] and as was recently reported by Ermolaev et al., MoS$_2$ nanosheets exhibit large optical anisotropy and birefringence between the basal plane and the nanosheets' edges.[27] Hence, it is clear that many applications require or can benefit from control over the orientation of the 2D-material.

The broad chemical variety of thermotropic liquid crystals (LCs) and the ability to readily control their orientation and ordering using external fields and surface-induced effects make them ideal candidates as mesophases for nanomaterial assembly.[28,29] Moreover, an additional level of functionality can be attained by combining the response of LCs to external stimuli (e.g., electric or magnetic fields) with anisotropic
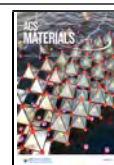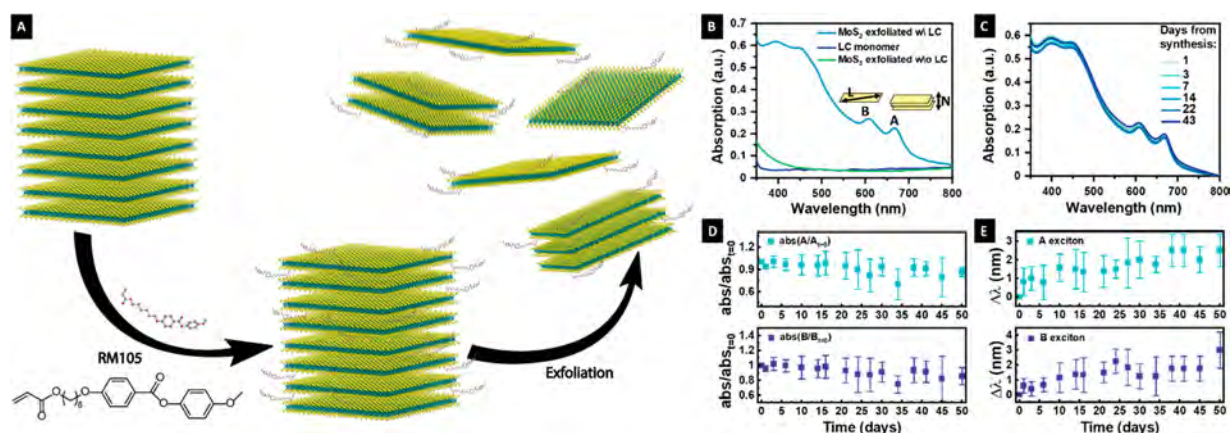
Figure 1. (A) Schematic illustration of MoS$_2$ exfoliation using thermotropic LCs. (B) Optical extinction spectra of MoS$_2$ suspensions produced with different exfoliation conditions. (C) Optical extinction spectra of the mesogen-containing-2D-MoS$_2$ suspension over time. (D) Relative intensity and (E) spectral shift at the A and B excitonic transition peaks over time.

properties of select nanomaterials to yield adaptive devices or materials.[29,30]

However, the challenges involved with a stable dispersion of nanomaterials (0D, 1D, and 2D) in such systems are nontrivial, as reported.[31−34] There are several examples of a stable MoS$_2$ dispersion in organic solvents[35−38] and its functionalization with organic ligands.[39−42] These reports mainly discuss either direct covalent functionalization of MoS$_2$ by organic ligands containing various functional groups such as thiols,[39] halides,[40] and diazonium salts[41] or, on the other hand, surfactant assisted exfoliation.[43,44] At this point there have been several reports highlighting efficacious methods for liquid phase exfoliation of MoS$_2$ resulting in high-quality single- and few-nanosheet dispersions. While the stability of nanomaterials in simple fluids (e.g., water, organic solvents) can be secured using a variety of surface-active species, ensuring stability in structured fluids (i.e., nematic, or smectic liquid crystals) is challenging due to nanomaterials' distortion of the fluid's director field by the nanomaterials, and their tendency to aggregate to minimize that deformation.[45−47] Concerning MoS$_2$ in particular, we are unaware of any successful examples of a stable dispersion in thermotropic LCs. The question arises as to whether the best way to do this is to use a mesogenic exfoliant to begin with.

Recent work by Jalili et. al[48] demonstrated that suspensions of MoS$_2$ nanosheets in water may form a nematic phase, similar to what was shown previously for graphene oxide.[49] In addition, prior studies have investigated the anchoring and assembly of nCB mesogens on the surface of bulk MoS$_2$ crystals.[50−52] Despite evidence of favorable interactions between nCB mesogens and bulk MoS$_2$ surfaces, a dispersion of MoS$_2$ nanosheets in nCBs (or any other) mesophase has not been demonstrated. Dispersions of MoS$_2$ nanosheets in thermotropic LCs, which are independent of nanosheet concentration, size, and solvent, as in a lyotropic phase, would open possibilities for orientation control of MoS$_2$ and the study of the nanosheets' anisotropic properties and enable technologies that rely and utilize this anisotropy more readily.

Here, we report the successful generation of nanocomposites of MoS$_2$ in thermotropic LCs. The strategy relies on the use of mesogenic species as exfoliants themselves. We identify a small number of moieties that act to facilitate the exfoliation and dispersion of MoS$_2$ in bulk solution and thereafter provide ordered fluidic media that sustain the dispersion of single-/few-sheet MoS$_2$. Dispersion is observed not just in the nematic and

isotropic fluids but also in the solid crystal and polymerized forms of the system.

MoS$_2$ was exfoliated mechanically in a mesogen-containing organic solvent, as depicted in Figure 1A. Briefly, a molar excess of RM105 and bulk MoS$_2$ microparticles were mixed under N$_2$ at 75 °C to promote mesogen interaction with MoS$_2$. The mixture was then sonicated in a nonpolar solvent (1,2-dichlorobenzene), with nonexfoliated material subsequently separated by centrifugation. An olive-green solution resulted, indicating successful exfoliation of (2H) 2D-MoS$_2$ (Figure S1). A detailed description of the experimental procedure can be found in the Experimental Methods section. The typical sheet concentration in solution was calculated to be 5.3 ± 0.6 μg/mL, using optical attenuation.[53] To confirm the presence of few-layered MoS$_2$ sheets, the extinction spectrum of the solution was obtained, revealing a characteristic spectrum for 2H-MoS$_2$ exhibiting the excitonic A and B transitions at ∼670 and ∼610 nm, respectively.[13] This spectrum did not appear when the bulk material was sonicated in the absence of the LC ligand (Figure 1B), indicating that the LC ligand is necessary to achieve successful exfoliation in the nonpolar solvent. The dispersion appeared stable, without any visible signs of aggregation for weeks, as can also be inferred upon examination of the evolution of the extinction spectrum over time (Figure 1C). 43 days following the synthesis, the UV−vis spectra of the suspension revealed only a marginal decrease in the intensity of the extinction peaks, indicating that the exfoliated MoS$_2$ sheets remained stably dispersed without significant aggregation and/or restacking of the 2D-sheets (Figure 1C,D). The positions of the A and B excitonic transitions are well-correlated to the number of layers and lateral size (respectively) of exfoliated MoS$_2$ sheets.[54] Changes in the peak positions over time can be used therefore to track increases of particle size due to restacking and/or aggregation.

Over a long period of time (>30 days), no significant shift in position of these peaks was observed, which indicates that little aggregation occurred in the suspensions (Figure 1E). In addition, dispersion stability was also demonstrated by redispersion of the sheets into other common solvents (Figure S1B). Overall, the minimal changes (in both peak intensity and position) over an extended period of time (>30 days) highlight the considerable stability of the sheets against aggregation and restacking.

MoS_2 nanosheets were deposited on substrates by drop-casting from the dilute suspensions and observed by atomic force microscopy (AFM) to determine the lateral dimensions and thicknesses of discrete sheets. Representative AFM height images of the exfoliated sheets can be seen in Figure 2A.
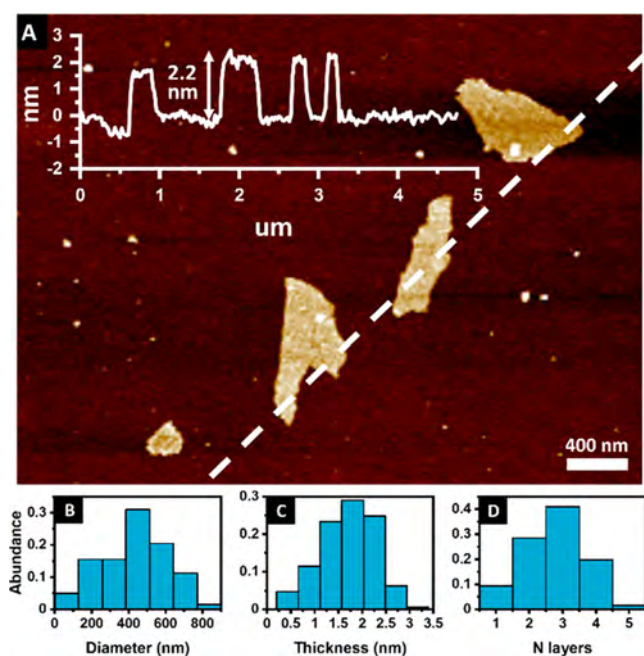
Figure 2. (A) AFM height image and profile of 2D-MoS_2 sheets drop-cast from solution. Distribution of exfoliated sheets' (B) size, (C) thickness, and (D) estimated number of layers.

Lateral size and thickness distributions indicate an average of ~430 ± 170 and 1.7 ± 0.5 nm, respectively (Figure 2B,C), which correlates to ~2−3-layer MoS_2 (Figure 2D).[3] Data from dynamic light scattering (DLS) measurements were in rough agreement, with a hydrodynamic diameter of 320 ± 50 nm (with a PDI of 0.32, Figure S2) inferred from the diffusive motion of the sheets. Sheets of varying sizes and thicknesses can be selectively separated with different centrifugation speeds, as inferred from the blue-shift of the A and B excitonic transition-related peaks upon increased centrifugation speeds (Figure S3).

In view of the desire to utilize MoS_2 in thin films and composites, we examined the stability of the exfoliated sheets in solid crystalline films produced by complete solvent evaporation from the suspensions, the nematic fluid produced at elevated temperatures from such films, and the polymer films produced by cross-linking such nematic fluids. The phase transition temperatures were determined by DSC (Figure S4). Raman spectroscopy was used to evaluate the presence of exfoliated sheet film samples. For 2D-MoS_2, the wavenumber difference between the E^1_{2g} and A_{1g} vibrational modes becomes smaller as the number of layers decreases, thereby differentiating between few-layer and bulk or restacked MoS_2.[55] Upon examination of the crystalline film at room temperature, the wavenumber difference was found to be 21 ± 2 cm^{-1}, which is substantially smaller than the difference measured for the bulk powder: 27.3 ± 0.6 cm^{-1} (Figure 3A). A difference of 6 cm^{-1} between the bulk MoS_2 powder and the exfoliated MoS_2 containing LC indicates that the sheets remained exfoliated, without significant aggregation.[36,55] The exact number of layers cannot be determined quantitatively from the measurement, due to effects caused by the presence of the organic ligand and excess LC surrounding the 2D sheets. However, the reduction in wavenumber difference is sufficiently large to indicate the existence of few-layer MoS_2,[36,56] which is consistent with the AFM data.

Temperature-resolved Raman measurements were used to examine the system in the nematic state. Similar to the room-temperature measurements, the wavenumber difference between the E^1_{2g} and A_{1g} modes, 23 ± 1 cm^{-1}, is lower than for bulk MoS_2, indicating that the nanosheets maintain their dispersion in the nematic state. This behavior was unchanged over multiple heating and cooling cycles (Figure S5). A histogram of the wavenumber differences measured across multiple sample positions in the crystal and nematic phases of the LC-MoS_2 composite highlights the presence of few-layer MoS_2 throughout the sample (Figure 3C).

RM105 is a reactive mesogen and can be polymerized to form a liquid crystal polymer (LCP) on its own, or a liquid crystal elastomer (LCE), when polymerized in tandem with other reactive mesogens or moieties that serve to lightly cross-link the material. The shape memory effect of aligned LCE and the anisotropic photothermal response of MoS_2 nanosheets suggest intriguing possibilities for the design of adaptive materials.[57,58] From this perspective, we examined the ability
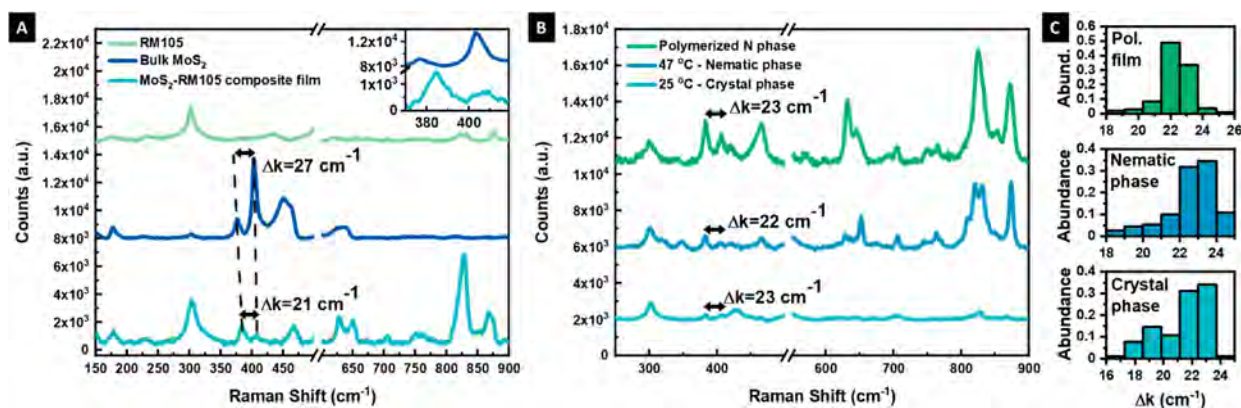
Figure 3. (A) Raman spectra of a solution cast film of MoS_2−RM105, bulk MoS_2, and RM105. (B) Raman spectra of different phases of the MoS_2−RM105 composite: crystal, nematic, and polymerized film. (C) Distribution of frequency differences between the E^1_{2g} and A_{1g} Raman modes of MoS_2 in the different phases.

to retain the nanosheet dispersion upon polymerization of the composite. The composite was mixed with a photoinitiator and polymerized by UV-light exposure (experimental details can be found in the Experimental Methods section). A green film was produced, indicating the presence of 2D-MoS_2 sheets. The color is in stark contrast to the pale-yellow color of polymerized RM105 without MoS_2 (Figure 4B, inset). The
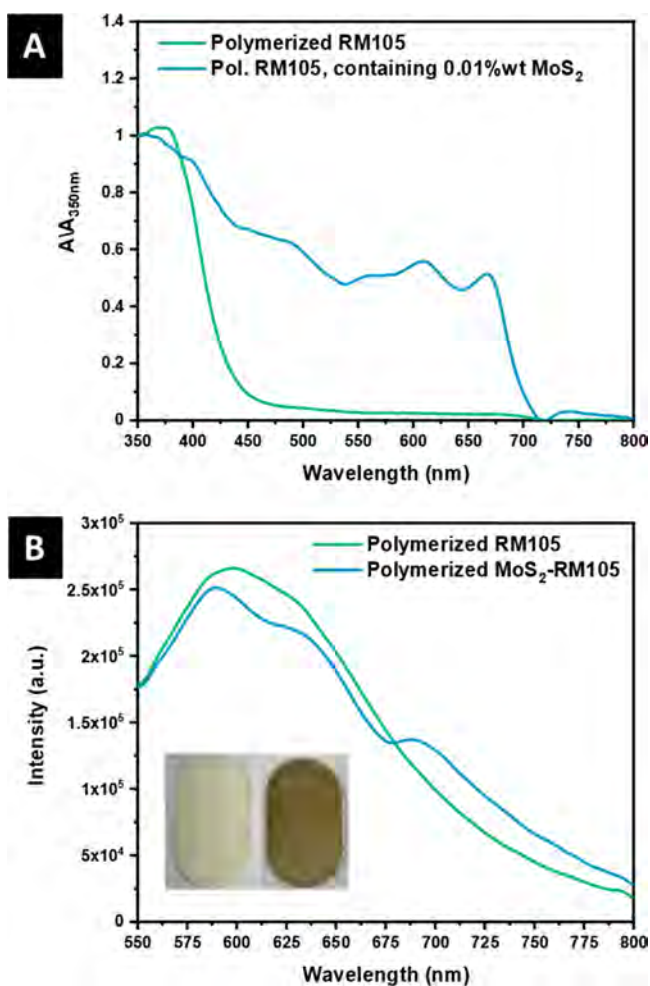
Figure 4. (A) Normalized absorption spectra of polymerized RM105 films, excluding and containing MoS_2. (B) PL spectra of the same MoS_2−RM105 films measured in part A. Inset: picture of the polymerized films.

presence of the 2D-sheets was confirmed by UV−vis absorption, which included the characteristic A and B excitonic transitions (Figure 4A). Additionally, upon measurements of the photoluminescence (PL) spectrum of the sample, PL peaks are observed at ~690 and ~630 nm, which correspond to the aforementioned A and B absorption transitions, respectively (Figure 4B). Raman spectra taken from the polymer film displayed a wavenumber difference of 22 ± 1 cm^{-1}, also indicating a retention of nanosheet dispersion after polymerization (Figure 3B,C), and consistent with the optical properties typical for few-layer MoS_2, distinct from the bulk material (Figure 4, Figure S6). Additionally, upon examination of the nanocomposite's structure by X-ray scattering, no signal relating to interlayer spacing of MoS_2 is apparent. This is in stark contrast to bulk MoS_2, where the restacking peak[3] (1.01 A^{-1}, 0.62 nm; see Figure S7) is prominent. The difference

indicates that there is no significant aggregation or restacking of MoS_2 in the polymer nanocomposite and supports the presence of few-layer MoS_2 nanosheets, as also evidenced by the optical characterization of the nanocomposite polymer film (see Figure 4).

RM105 is clearly efficacious in dispersing mechanically exfoliated 2D-sheets of MoS_2. We examined whether a similar efficacy could be obtained with other mesogens. Exfoliation was carried out using two other cross-linkable LCs with a similar chemical structure to RM105: RM82 (1,4-bis-[4-(6-acryloyloxyhexyloxy)benzoyloxy]-2-methylbenzene) and 6OBA (4-((6-(acryloyloxy)hexyl)oxy)benzoic acid). Exfoliation was performed in a similar fashion as with RM105. Green suspensions resulted in both cases, indicating the presence of few-layer MoS_2. Absorption measurements of the dispersions show spectra characteristic of MoS_2 (Figure S8B). Time-resolved studies suggested that RM82 was similarly efficacious as RM105, while 6OBA was somewhat less effective in preventing aggregation over time (Figure S8C,D). Mechanical exfoliation in the presence of cyanobiphenyl (CB)-based mesogens, viz. RM23 (4′-cyano-[1,1′-biphenyl]-4-yl 4-((6-(acryloyloxy)hexyl)oxy)benzoate), 5CB, 6OCB, and 8CB (4′-pentyl-, 4′-hexyloxy-, and 4′-octyl-4-biphenylcarbonitrile, respectively, see Figure S9), was unsuccessful. This was unexpected, as prior studies have highlighted the formation of kinked lamellar structures of nCB on MoS_2 crystals, driven by nominally favorable interactions and structural commensurabilities.[50−52,59]

There are several possibilities that may account for the observed differences in the exfoliation efficacies of the different mesogens. In the broadest terms, exfoliation and subsequent stabilization are favored by low sheet cohesion energy and a small interfacial tension between exfoliated sheets and the surrounding medium, respectively.[53,60] Several reports discussed optimization of solubility parameters[53] or surface tension components[61,62] to minimize these terms. This suggests that molecular species that exfoliate (and subsequently disperse) nanosheets should have favorable interactions with the sheet surface. One therefore anticipates that species that are more efficacious in nanosheet exfoliation would have more favorable interactions with MoS_2 than species which are less efficacious. These interactions could be manifested in the form of chemical bonding or nonbonded interactions such as electrostatic interactions. Upon examination of the MoS_2-containing RM105 and the pure LC by ^{1}H NMR, no significant changes were discernible in the proton spectra for RM105 (Figure S10), and so covalent bonding of RM105 to MoS_2 is considered unlikely. This is in line with expectations as sample preparation and subsequent MoS_2 exfoliation were performed under mild conditions that would not be expected to promote a chemical reaction, and also because RM105 does not have particularly labile functional groups. As RM105 is uncharged, and the system entails low polarity media, it is unlikely that electrostatics play a role in the mesogen−nanosheet interactions. It is also unlikely that hydrogen bonding plays a significant role given the absence of well-identified H-bond donors and acceptors in the system. We surmise that the interactions are dipole-based and as such that they may depend on the nature of the MoS_2 surface produced during exfoliation (e.g., presence of S-vacancies).

We used molecular dynamics simulations of two representative species to better understand the interactions between MoS_2 and the mesogenic species and probe whether there were

observable differences in their interactions with the MoS_2 surface (see details in the Experimental Methods section; Figure S11). The simulation, representing an RM105 droplet surrounded by 5CB on top of a MoS_2 surface, depicts the formation of an RM105 droplet with a contact angle θ_D of roughly 70°. As it is less than 90°, the contact angle indicates that the MoS_2 surface favors RM105 over 5CB, which is consistent with our experimental finding that RM105 was more efficacious than 5CB in exfoliating (and dispersing) MoS_2 nanosheets. These findings highlight the likelihood that surface tension plays an important role in the exfoliation of MoS_2 by mesogenic species, similar to what was reported with isotropic-solvent exfoliation.[53,61] Based on the experimental and simulation results, we can postulate that favorable surface interactions with MoS_2 are sufficient to make RM105 an efficacious exfoliant, while the interactions of 5CB with MoS_2 are not favorable enough to drive exfoliation. The presence of a carbonitrile group is common among the mesogens that were not successful in exfoliating nanosheets. Indeed, the difference between RM105 and RM23 is the substitution of a methoxy group on RM105 by a carbonitrile group on RM23 (see Figure S9). We speculate that the polarity of the −CN group reduces the favorability of the interaction with MoS_2 to a large enough extent that the CN-bearing mesogens are ineffective in dispersing exfoliated nanosheets. Studies that focus specifically on elucidating the mesogen−nanosheet interactions and the interactions of mesogen-ligated nanosheets in solution are needed. Such studies may provide more insight regarding differences in dispersion efficacy and identify the molecular underpinnings of the long-lived dispersion stability observed in these systems. Further, they may shed light on whether the mesogens intercalate MoS_2 or otherwise play a role in the exfoliation process itself.

In summary, we present a method to simultaneously exfoliate and disperse MoS_2 nanosheets in a thermotropic LC. 2D-MoS_2 was exfoliated in a solution containing a mesogenic species after mild sonication. A stable dispersion was demonstrated by examination of the extinction spectra of the solution, with signs of only minor aggregation over prolonged periods of time. Stability of the 2D material dispersion was also observed in cast films by temperature-resolved Raman spectroscopy. The wavenumber difference between two characteristic modes of 2D-MoS_2 was significantly reduced in the 2D-LC composite compared to the bulk MoS_2, in both the crystal and nematic phases, indicating a stable dispersion of the sheets over a wide range of temperatures. Stability of the 2D sheets was also examined in polymerized RM105. Characteristic optical extinction, PL, and Raman spectra establish the presence of well-dispersed single-/few-layer MoS_2 in the resulting LC polymer. These results conclusively demonstrate a stable dispersion of 2D-MoS_2 in a thermotropic LC and suggest a broad range of new possibilities for the study of MoS_2 nanocomposites and the design of functional materials.

■ EXPERIMENTAL METHODS

Materials. 4-Methoxyphenyl 4-((6-(acryloyloxy)hexyl)-oxy)benzoate, 97% (RM105); 2-methyl-1,4-phenylene bis(4-((6-(acryloyloxy)hexyl)oxy)benzoate), 95% (RM82); and 4-((6-(acryloyloxy)hexyl)oxy)benzoic acid, 97% (6OBA), were purchased from AmBeed Chemicals. MoS_2 (powder, 98%, particle size <2 μm), phenylbis(2,4,6-trimethylbenzoyl)-phosphine oxide (IrgaCure 819, 97%), and 1,2-dichlorobenzne

(DCB, 99%) were purchased from Sigma-Aldrich. All chemicals were used as bought without any further purification.

MoS_2 Exfoliation into RM105. Exfoliation of MoS_2 with LCs has been adapted from previous reports on exfoliation with non-LC ligands.[36,63] In a typical synthesis, RM105 was mixed with MoS_2 powder in a 1.55:1 stoichiometric balance. The reaction vessel was purged with nitrogen and placed in an oil bath at 75 °C for 24 h, after which it was taken out and allowed to cool to room temperature. Next, DCB was added to keep MoS_2 at a concentration of 10 mg/mL, and the vessel was purged with nitrogen again. Exfoliation was performed using continuous sonication in an ultrasonic bath (Branson 250) for 6 h, and separation of unexfoliated material was done using centrifugation (VWR clinical 200 centrifuge) at 3000 rpm (1100 rcf) twice.

Film Casting for Raman Measurements. For Raman measurements, a dry film was prepared by drop casting the solution containing the exfoliated sheets on a precleaned Si wafer, followed by solvent removal by evaporation at 140 °C.

Photopolymerization of the MoS_2−RM105 Composite. After evaporation of DCB, the resulting dry material was redispersed in chloroform, to which 1 wt % of the photoinitiator Irgacure 819 was added. Next, the solution was cast into a mold on top of a glass substrate and the solvent removed by evaporation on a hot plate. To polymerize at the nematic phase, the resulting cast film was heated to 140 °C and then immediately transferred under a UV lamp (sunspot 2, 100 W) in a chamber purged with N_2. The lamp was then turned, and the film was exposed to UV light for 15 min.

Characterization. UV−vis spectra were collected in a Cary 100 bio instrument; AFM images were taken using a Bruker Icon AFM instrument, and Raman was measured using a Horiba LabRam Evolution confocal Raman microscope, using 633 nm light excitation and 120 s exposure under a 100× objective. For temperature-resolved Raman spectroscopy, the sample was placed on top of a Linkam hot stage and scanned using a 50× objective. PL spectra were collected using an Edinburgh instruments FLS1000 fluorometer with an excitation light of 532 nm. Thermal analysis data were collected using a TA DSC 2500 instrument. POM imaging was performed using a Zeiss Axio Observer microscope equipped with cross polarizers and equipped with a Pike CCD camera. DLS measurements were taken using a Brookhaven BI-200SM instrument with a Compact red laser diode with 40 mW power and 640 nm wavelength. ^{1}H NMR spectra of RM105 and MoS_2 containing RM105 were collected from a Bruker AVII 500 spectrometer using deuterated chloroform ($CDCl_3$) as the solvent.

Molecular Models and Simulation Details. MoS_2 surfaces were modeled using position-restrained Lennard-Jones atoms with parameters obtained from Luan and Zhou[64] using harmonic springs with a spring constant of 10^5 kJmol^{-1} nm^{-2}. This model has been shown to accurately estimate the contact angles for H_2O and isopropyl alcohol mixtures on MoS_2 at a variety of concentrations.[65] 5CB was modeled using the AMBER-based united atom force field described by Tiberio et al.[66] which accurately captures the complex phase behavior of the nCB series of mesogens in addition to their bulk properties. RM105 was modeled using the GAFF-LC force field created by Boyd and Wilson, which modifies several dihedrals and Lennard-Jones parameters from GAFF to better capture isotropic−nematic transitions in bent-core mesogens

and mesogens with phenyl benzoate moieties.[67,68] We have tested the applicability of the GAFF-LC model for RM105 and find that it undergoes an isotropic-to-nematic transition near the temperature expected from experiments.

All simulations were performed using GROMACS 2020.5.[69,70] A cutoff distance of $r_{cut} = 1.2$ nm was used for all short-ranged interactions. Lennard-Jones cross-interactions were computed using the Lorentz−Berthelot combination rules, and reciprocal space electrostatics were computed using the particle mesh Ewald summation[71] with a Fourier spacing of 0.12 nm. The equations of motion are integrated using the leapfrog algorithm with a time-step of 2 fs. All simulations were performed in the NPT ensemble. The stochastic velocity-rescale thermostat[72] was used with a time constant of 0.5 ps to maintain the temperature at 400 K. Pressure was maintained at 1 bar using the Berensden[73] (time constant of 5 ps) and Parinello−Rahman[74] (time constant of 100 ps) barostats during the equilibration and production runs, respectively. Hydrogen bonds were constrained using the LINCS[75] algorithm.

To prevent the mixing of RM105 and 5CB when conducting droplet simulations, Lennard-Jones cross-interaction energies between the molecules were scaled by a parameter $\alpha = 0.8$. This decrease in the effective interactions between the mesogens prevents them from mixing with one another and ought to also increase the surface tension between them. The mesogen−surface interactions were not scaled or altered in any way.

MoS$_2$ sheets were visualized using Vesta software.[78]

Droplet Simulations for Estimating Contact Angles. To determine whether a MoS$_2$ surface prefers RM105 or 5CB, simulation of an infinitely long cylindrical droplet consisting of 100 RM105 molecules surrounded by 500 5CB molecules was performed. The molecules are placed on a position-restrained MoS$_2$ surface consisting of 4608 atoms arranged in a $13.2 \times 5.1 \times 1.5$ nm plate. The system is equilibrated in the NPT ensemble for 12 ns at $T = 400$ K and $P = 1$ bar using the stochastic velocity-rescaling thermostat and Berendsen barostat with anisotropic pressure coupling such that the system can only change volume in the z-direction. A production run of 100 ns is performed using the same system setup, with the Parinello−Rahman barostat being used in lieu of the Berendsen barostat. The configurations are collected every 5 ps and are averaged to generate a 2D histogram of RM105 density in the $x−z$ plane. The half-density isosurface is calculated and is fitted with a circle to estimate the corresponding contact angle, θ_D. This analysis was performed using the Python library MDAnalysis,[76] and simulation snapshots are shown using VMD.[77]

■ ASSOCIATED CONTENT

Ⓢ Supporting Information

The Supporting Information is available free of charge at https://pubs.acs.org/doi/10.1021/acsmaterialslett.1c00222.

> Additional spectroscopy data (UV−vis, Raman); polarized optical micrographs of LC dispersions; photographs of MoS$_2$ suspensions; X-ray scattering; NMR data; and simulation results (PDF)

■ AUTHOR INFORMATION

Corresponding Author

Chinedum O. Osuji − *Department of Chemical and Biomolecular Engineering, University of Pennsylvania, Philadelphia, Pennsylvania 19104, United States; Department of Chemical and Environmental Engineering, Yale University, New Haven, Connecticut 06511, United States;* ⓘ orcid.org/0000-0003-0261-3065; Email: cosuji@seas.upenn.edu

Authors

Uri R. Gabinet − *Department of Chemical and Biomolecular Engineering, University of Pennsylvania, Philadelphia, Pennsylvania 19104, United States; Department of Chemical and Environmental Engineering, Yale University, New Haven, Connecticut 06511, United States*

Changyeon Lee − *Department of Chemical and Biomolecular Engineering, University of Pennsylvania, Philadelphia, Pennsylvania 19104, United States*

Ryan Poling-Skutvik − *Department of Chemical and Biomolecular Engineering, University of Pennsylvania, Philadelphia, Pennsylvania 19104, United States; Department of Chemical Engineering, University of Rhode Island, Kingston, Rhode Island 02881, United States;* ⓘ orcid.org/0000-0002-1614-1647

Daniel Keane − *Department of Chemical Engineering, University of Rhode Island, Kingston, Rhode Island 02881, United States*

Na Kyung Kim − *Department of Chemical and Biomolecular Engineering, University of Pennsylvania, Philadelphia, Pennsylvania 19104, United States*

Ruiqi Dong − *Department of Chemical and Biomolecular Engineering, University of Pennsylvania, Philadelphia, Pennsylvania 19104, United States*

Zachariah Vicars − *Department of Chemical and Biomolecular Engineering, University of Pennsylvania, Philadelphia, Pennsylvania 19104, United States*

Yusheng Cai − *Department of Chemical and Biomolecular Engineering, University of Pennsylvania, Philadelphia, Pennsylvania 19104, United States*

Aniket U. Thosar − *Department of Chemical and Biomolecular Engineering, University of Pennsylvania, Philadelphia, Pennsylvania 19104, United States*

Alexander Grun − *Department of Materials Science and Engineering, University of Pennsylvania, Philadelphia, Pennsylvania 19104, United States*

Sarah M. Thompson − *Department of Electrical and Systems Engineering, University of Pennsylvania, Philadelphia, Pennsylvania 19104, United States*

Amish J. Patel − *Department of Chemical and Biomolecular Engineering, University of Pennsylvania, Philadelphia, Pennsylvania 19104, United States;* ⓘ orcid.org/0000-0001-6482-543X

Cherie R. Kagan − *Department of Materials Science and Engineering, Department of Electrical and Systems Engineering, and Department of Chemistry, University of Pennsylvania, Philadelphia, Pennsylvania 19104, United States;* ⓘ orcid.org/0000-0001-6540-2009

Russell J. Composto − *Department of Materials Science and Engineering, University of Pennsylvania, Philadelphia, Pennsylvania 19104, United States;* ⓘ orcid.org/0000-0002-5906-2594

Complete contact information is available at:

https://pubs.acs.org/10.1021/acsmaterialslett.1c00222

Author Contributions

The manuscript was written through contributions of all authors.

Notes

The authors declare no competing financial interest.

■ ABBREVIATIONS

LC   liquid crystal
LCP   liquid crystal polymer
LCE   liquid crystal elastomer
TMDs transition metal dichalcogenides
AFM   atomic force microscopy
DLS   dynamic light scattering
PDI   polydispersity index
DSC   differential scanning calorimetry
POM   polarized optical microscopy

■ REFERENCES

(1) Allen, M. J.; Tung, V. C.; Kaner, R. B. Honeycomb Carbon: A Review of Graphene. *Chem. Rev.* **2010**, *110*, 132−145.

(2) Novoselov, K. S.; Mishchenko, A.; Carvalho, A.; Castro Neto, A. H. 2D materials and van der Waals heterostructures. *Science* **2016**, *353*, aac9439.

(3) Venkata Subbaiah, Y. P.; Saji, K. J.; Tiwari, A. Atomically Thin MoS2: A Versatile Nongraphene 2D Material. *Adv. Funct. Mater.* **2016**, *26*, 2046−2069.

(4) Akhtar, M.; Anderson, G.; Zhao, R.; Alruqi, A.; Mroczkowska, J. E.; Sumanasekera, G.; Jasinski, J. B. Recent advances in synthesis, properties, and applications of phosphorene. *npj 2D Mater. Appl.* **2017**, *1*, 5.

(5) Donarelli, M.; Ottaviano, L. 2D Materials for Gas Sensing Applications: A Review on Graphene Oxide, MoS2, WS2 and Phosphorene. *Sensors* **2018**, *18*, 3638.

(6) Ranjan, P.; Lee, J. M.; Kumar, P.; Vinu, A. Borophene: New Sensation in Flatland. *Adv. Mater.* **2020**, *32*, 2000531.

(7) Tan, C.; Cao, X.; Wu, X.-J.; He, Q.; Yang, J.; Zhang, X.; Chen, J.; Zhao, W.; Han, S.; Nam, G.-H.; Sindoro, M.; Zhang, H. Recent Advances in Ultrathin Two-Dimensional Nanomaterials. *Chem. Rev.* **2017**, *117*, 6225−6331.

(8) Han, G. H.; Duong, D. L.; Keum, D. H.; Yun, S. J.; Lee, Y. H. van der Waals Metallic Transition Metal Dichalcogenides. *Chem. Rev.* **2018**, *118*, 6297−6336.

(9) Wang, H.; Li, C.; Fang, P.; Zhang, Z.; Zhang, J. Z. Synthesis, properties, and optoelectronic applications of two-dimensional MoS2 and MoS2-based heterostructures. *Chem. Soc. Rev.* **2018**, *47*, 6101−6127.

(10) Kang, K.; Xie, S.; Huang, L.; Han, Y.; Huang, P. Y.; Mak, K. F.; Kim, C.-J.; Muller, D.; Park, J. High-mobility three-atom-thick semiconducting films with wafer-scale homogeneity. *Nature* **2015**, *520*, 656−660.

(11) Duerloo, K.-A. N.; Li, Y.; Reed, E. J. Structural phase transitions in two-dimensional Mo- and W-dichalcogenide monolayers. *Nat. Commun.* **2014**, *5*, 4214.

(12) Mak, K. F.; Lee, C.; Hone, J.; Shan, J.; Heinz, T. F. Atomically Thin MoS$_2$: A New Direct-Gap Semiconductor. *Phys. Rev. Lett.* **2010**, *105*, 136805.

(13) Splendiani, A.; Sun, L.; Zhang, Y.; Li, T.; Kim, J.; Chim, C.-Y.; Galli, G.; Wang, F. Emerging Photoluminescence in Monolayer MoS2. *Nano Lett.* **2010**, *10*, 1271−1275.

(14) Li, D.; Xiong, W.; Jiang, L.; Xiao, Z.; Rabiee Golgir, H.; Wang, M.; Huang, X.; Zhou, Y.; Lin, Z.; Song, J.; Ducharme, S.; Jiang, L.; Silvain, J.-F.; Lu, Y. Multimodal Nonlinear Optical Imaging of MoS2 and MoS2-Based van der Waals Heterostructures. *ACS Nano* **2016**, *10*, 3766−3775.

(15) Yin, X.; Ye, Z.; Chenet, D. A.; Ye, Y.; O'Brien, K.; Hone, J. C.; Zhang, X. Edge Nonlinear Optics on a MoS$_2$ Atomic Monolayer. *Science* **2014**, *344*, 488−490.

(16) Zhang, X.; Zhang, S.; Xie, Y.; Huang, J.; Wang, L.; Cui, Y.; Wang, J. Tailoring the nonlinear optical performance of two-dimensional MoS2 nanofilms via defect engineering. *Nanoscale* **2018**, *10*, 17924−17932.

(17) Lei, Z.; Zhan, J.; Tang, L.; Zhang, Y.; Wang, Y. Recent Development of Metallic (1T) Phase of Molybdenum Disulfide for Energy Conversion and Storage. *Adv. Energy Mater.* **2018**, *8*, 1703482.

(18) Liu, H.; Su, D.; Zhou, R.; Sun, B.; Wang, G.; Qiao, S. Z. Highly Ordered Mesoporous MoS2 with Expanded Spacing of the (002) Crystal Plane for Ultrafast Lithium Ion Storage. *Adv. Energy Mater.* **2012**, *2*, 970−975.

(19) Acerce, M.; Voiry, D.; Chhowalla, M. Metallic 1T phase MoS2 nanosheets as supercapacitor electrode materials. *Nat. Nanotechnol.* **2015**, *10*, 313−318.

(20) Li, Y.; Wang, H.; Xie, L.; Liang, Y.; Hong, G.; Dai, H. MoS2 Nanoparticles Grown on Graphene: An Advanced Catalyst for the Hydrogen Evolution Reaction. *J. Am. Chem. Soc.* **2011**, *133*, 7296−7299.

(21) Voiry, D.; Salehi, M.; Silva, R.; Fujita, T.; Chen, M.; Asefa, T.; Shenoy, V. B.; Eda, G.; Chhowalla, M. Conducting MoS2 Nanosheets as Catalysts for Hydrogen Evolution Reaction. *Nano Lett.* **2013**, *13*, 6222−6227.

(22) Wang, H.; Lu, Z.; Xu, S.; Kong, D.; Cha, J. J.; Zheng, G.; Hsu, P.-C.; Yan, K.; Bradshaw, D.; Prinz, F. B.; Cui, Y. Electrochemical tuning of vertically aligned MoS$_2$ nanofilms and its application in improving hydrogen evolution reaction. *Proc. Natl. Acad. Sci. U. S. A.* **2013**, *110*, 19701−19706.

(23) Cho, S.-Y.; Kim, S. J.; Lee, Y.; Kim, J.-S.; Jung, W.-B.; Yoo, H.-W.; Kim, J.; Jung, H.-T. Highly Enhanced Gas Adsorption Properties in Vertically Aligned MoS2 Layers. *ACS Nano* **2015**, *9*, 9314−9321.

(24) Hirunpinyopas, W.; Prestat, E.; Worrall, S. D.; Haigh, S. J.; Dryfe, R. A. W.; Bissett, M. A. Desalination and Nanofiltration through Functionalized Laminar MoS2Membranes. *ACS Nano* **2017**, *11*, 11082−11090.

(25) Wang, G.; Zhang, J.; Yang, S.; Wang, F.; Zhuang, X.; Müllen, K.; Feng, X. Vertically Aligned MoS2 Nanosheets Patterned on Electrochemically Exfoliated Graphene for High-Performance Lithium and Sodium Storage. *Adv. Energy Mater.* **2018**, *8*, 1702254.

(26) Bolhuis, M.; Hernandez-Rueda, J.; van Heijst, S. E.; Tinoco Rivas, M.; Kuipers, L.; Conesa-Boj, S. Vertically-oriented MoS2 nanosheets for nonlinear optical devices. *Nanoscale* **2020**, *12*, 10491−10497.

(27) Ermolaev, G. A.; Grudinin, D. V.; Stebunov, Y. V.; Voronin, K. V.; Kravets, V. G.; Duan, J.; Mazitov, A. B.; Tselikov, G. I.; Bylinkin, A.; Yakubovsky, D. I.; Novikov, S. M.; Baranov, D. G.; Nikitin, A. Y.; Kruglov, I. A.; Shegai, T.; Alonso-González, P.; Grigorenko, A. N.; Arsenin, A. V.; Novoselov, K. S.; Volkov, V. S. Giant optical anisotropy in transition metal dichalcogenides for next-generation photonics. *Nat. Commun.* **2021**, *12*, 854.

(28) Zhang, S.; Pelligra, C. I.; Feng, X.; Osuji, C. O. Directed Assembly of Hybrid Nanomaterials and Nanocomposites. *Adv. Mater.* **2018**, *30*, 1705794.

(29) Gabinet, U. R.; Osuji, C. O. Optical materials and metamaterials from nanostructured soft matter. *Nano Res.* **2019**, *12*, 2172−2183.

(30) Zhang, Y.; Liu, Q.; Mundoor, H.; Yuan, Y.; Smalyukh, I. I. Metal Nanoparticle Dispersion, Alignment, and Assembly in Nematic

Liquid Crystals for Applications in Switchable Plasmonic Color Filters and E-Polarizers. *ACS Nano* **2015**, *9*, 3097−3108.

(31) Atorf, B.; Funck, T.; Hegmann, T.; Kempter, S.; Liedl, T.; Martens, K.; Mühlenbernd, H.; Zentgraf, T.; Zhang, B.; Kitzerow, H.; Urbanski, M. Liquid crystals and precious metal: from nanoparticle dispersions to functional plasmonic nanostructures. *Liq. Cryst.* **2017**, *44*, 1929−1947.

(32) Saliba, S.; Mingotaud, C.; Kahn, M. L.; Marty, J.-D. Liquid crystalline thermotropic and lyotropic nanohybrids. *Nanoscale* **2013**, *5*, 6641−6661.

(33) Bisoyi, H. K.; Kumar, S. Liquid-crystal nanoscience: an emerging avenue of soft self-assembly. *Chem. Soc. Rev.* **2011**, *40*, 306−319.

(34) Draper, M.; Saez, I. M.; Cowling, S. J.; Gai, P.; Heinrich, B.; Donnio, B.; Guillon, D.; Goodby, J. W. Self-Assembly and Shape Morphology of Liquid Crystalline Gold Metamaterials. *Adv. Funct. Mater.* **2011**, *21*, 1260−1278.

(35) Chou, S. S.; Huang, Y.-K.; Kim, J.; Kaehr, B.; Foley, B. M.; Lu, P.; Dykstra, C.; Hopkins, P. E.; Brinker, C. J.; Huang, J.; Dravid, V. P. Controlling the Metal to Semiconductor Transition of MoS2 and WS2 in Solution. *J. Am. Chem. Soc.* **2015**, *137*, 1742−1745.

(36) Ahmad, R.; Srivastava, R.; Yadav, S.; Singh, D.; Gupta, G.; Chand, S.; Sapra, S. Functionalized Molybdenum Disulfide Nanosheets for 0D−2D Hybrid Nanostructures: Photoinduced Charge Transfer and Enhanced Photoresponse. *J. Phys. Chem. Lett.* **2017**, *8*, 1729−1738.

(37) Giovanelli, E.; Castellanos-Gomez, A.; Pérez, E. M. Surfactant-Free Polar-to-Nonpolar Phase Transfer of Exfoliated MoS2 Two-Dimensional Colloids. *ChemPlusChem* **2017**, *82*, 732−741.

(38) Tang, Z.; Wei, Q.; Guo, B. A generic solvent exchange method to disperse MoS2 in organic solvents to ease the solution process. *Chem. Commun.* **2014**, *50*, 3934−3937.

(39) Chou, S. S.; De, M.; Kim, J.; Byun, S.; Dykstra, C.; Yu, J.; Huang, J.; Dravid, V. P. Ligand Conjugation of Chemically Exfoliated MoS2. *J. Am. Chem. Soc.* **2013**, *135*, 4584−4587.

(40) Voiry, D.; Goswami, A.; Kappera, R.; Silva, C. d. C. C. e.; Kaplan, D.; Fujita, T.; Chen, M.; Asefa, T.; Chhowalla, M. Covalent functionalization of monolayered transition metal dichalcogenides by phase engineering. *Nat. Chem.* **2015**, *7*, 45−49.

(41) Knirsch, K. C.; Berner, N. C.; Nerl, H. C.; Cucinotta, C. S.; Gholamvand, Z.; McEvoy, N.; Wang, Z.; Abramovic, I.; Vecera, P.; Halik, M.; Sanvito, S.; Duesberg, G. S.; Nicolosi, V.; Hauke, F.; Hirsch, A.; Coleman, J. N.; Backes, C. Basal-Plane Functionalization of Chemically Exfoliated Molybdenum Disulfide by Diazonium Salts. *ACS Nano* **2015**, *9*, 6018−6030.

(42) Chen, X.; Berner, N. C.; Backes, C.; Duesberg, G. S.; McDonald, A. R. Functionalization of Two-Dimensional MoS2: On the Reaction Between MoS2 and Organic Thiols. *Angew. Chem., Int. Ed.* **2016**, *55*, 5803−5808.

(43) Smith, R. J.; King, P. J.; Lotya, M.; Wirtz, C.; Khan, U.; De, S.; O'Neill, A.; Duesberg, G. S.; Grunlan, J. C.; Moriarty, G.; Chen, J.; Wang, J.; Minett, A. I.; Nicolosi, V.; Coleman, J. N. Large-Scale Exfoliation of Inorganic Layered Compounds in Aqueous Surfactant Solutions. *Adv. Mater.* **2011**, *23*, 3944−3948.

(44) Gupta, A.; Arunachalam, V.; Vasudevan, S. Water Dispersible, Positively and Negatively Charged MoS2 Nanosheets: Surface Chemistry and the Role of Surfactant Binding. *J. Phys. Chem. Lett.* **2015**, *6*, 739−744.

(45) Liu, Q.; Yuan, Y.; Smalyukh, I. I. Electrically and Optically Tunable Plasmonic Guest−Host Liquid Crystals with Long-Range Ordered Nanoparticles. *Nano Lett.* **2014**, *14*, 4071−4077.

(46) Mertelj, A.; Lisjak, D.; Drofenik, M.; Čopič, M. Ferromagnetism in suspensions of magnetic platelets in liquid crystal. *Nature* **2013**, *504*, 237−241.

(47) Smalyukh, I. I. Liquid Crystal Colloids. *Annu. Rev. Condens. Matter Phys.* **2018**, *9*, 207−226.

(48) Jalili, R.; Aminorroaya-Yamini, S.; Benedetti, T. M.; Aboutalebi, S. H.; Chao, Y.; Wallace, G. G.; Officer, D. L. Processable 2D materials beyond graphene: MoS2 liquid crystals and fibres. *Nanoscale* **2016**, *8*, 16862−16867.

(49) Kim, J. E.; Han, T. H.; Lee, S. H.; Kim, J. Y.; Ahn, C. W.; Yun, J. M.; Kim, S. O. Graphene Oxide Liquid Crystals. *Angew. Chem., Int. Ed.* **2011**, *50*, 3043−3047.

(50) Lacaze, E.; Michel, J. P.; Goldmann, M.; Gailhanou, M.; Boissieu, M. d.; Alba, M. Bistable nematic and smectic anchoring in the liquid crystal octylcyanobiphenyl (8CB) adsorbed on a ${\mathrm{MoS}}_{2}$ single crystal. *Phys. Rev. E* **2004**, *69*, 041705.

(51) Hara, M.; Iwakabe, Y.; Tochigi, K.; Sasabe, H.; Garito, A. F.; Yamada, A. Anchoring structure of smectic liquid-crystal layers on MoS2 observed by scanning tunnelling microscopy. *Nature* **1990**, *344*, 228−230.

(52) Kim, D. W.; Ok, J. M.; Jung, W.-B.; Kim, J.-S.; Kim, S. J.; Choi, H. O.; Kim, Y. H.; Jung, H.-T. Direct Observation of Molybdenum Disulfide, MoS2, Domains by Using a Liquid Crystalline Texture Method. *Nano Lett.* **2015**, *15*, 229−234.

(53) Coleman, J. N.; Lotya, M.; O'Neill, A.; Bergin, S. D.; King, P. J.; Khan, U.; Young, K.; Gaucher, A.; De, S.; Smith, R. J.; Shvets, I. V.; Arora, S. K.; Stanton, G.; Kim, H.-Y.; Lee, K.; Kim, G. T.; Duesberg, G. S.; Hallam, T.; Boland, J. J.; Wang, J. J.; Donegan, J. F.; Grunlan, J. C.; Moriarty, G.; Shmeliov, A.; Nicholls, R. J.; Perkins, J. M.; Grieveson, E. M.; Theuwissen, K.; McComb, D. W.; Nellist, P. D.; Nicolosi, V. Two-Dimensional Nanosheets Produced by Liquid Exfoliation of Layered Materials. *Science* **2011**, *331*, 568−571.

(54) Backes, C.; Smith, R. J.; McEvoy, N.; Berner, N. C.; McCloskey, D.; Nerl, H. C.; O'Neill, A.; King, P. J.; Higgins, T.; Hanlon, D.; Scheuschner, N.; Maultzsch, J.; Houben, L.; Duesberg, G. S.; Donegan, J. F.; Nicolosi, V.; Coleman, J. N. Edge and confinement effects allow in situ measurement of size and thickness of liquid-exfoliated nanosheets. *Nat. Commun.* **2014**, *5*, 4576.

(55) Li, H.; Zhang, Q.; Yap, C. C. R.; Tay, B. K.; Edwin, T. H. T.; Olivier, A.; Baillargeat, D. From Bulk to Monolayer MoS2: Evolution of Raman Scattering. *Adv. Funct. Mater.* **2012**, *22*, 1385−1390.

(56) Guan, G.; Zhang, S.; Liu, S.; Cai, Y.; Low, M.; Teng, C. P.; Phang, I. Y.; Cheng, Y.; Duei, K. L.; Srinivasan, B. M.; Zheng, Y.; Zhang, Y.-W.; Han, M.-Y. Protein Induces Layer-by-Layer Exfoliation of Transition Metal Dichalcogenides. *J. Am. Chem. Soc.* **2015**, *137*, 6152−6155.

(57) Lei, Z.; Zhu, W.; Sun, S.; Wu, P. MoS2-based dual-responsive flexible anisotropic actuators. *Nanoscale* **2016**, *8*, 18800−18807.

(58) Hu, D.; Yang, X.; Li, C.; Liu, R.; Yao, Z.; Hu, H.; Corder, S. N. G.; Chen, J.; Sun, Z.; Liu, M.; Dai, Q. Probing optical anisotropy of nanometer-thin van der waals microcrystals by near-field imaging. *Nat. Commun.* **2017**, *8*, 1471.

(59) Lacaze, E.; Apicella, A.; De Santo, M. P.; Coursault, D.; Alba, M.; Goldmann, M.; Barberi, R. Ordered interfaces for dual easy axes in liquid crystals. *Soft Matter* **2011**, *7*, 1078−1083.

(60) Tao, H.; Zhang, Y.; Gao, Y.; Sun, Z.; Yan, C.; Texter, J. Scalable exfoliation and dispersion of two-dimensional materials − an update. *Phys. Chem. Chem. Phys.* **2017**, *19*, 921−960.

(61) Shen, J.; He, Y.; Wu, J.; Gao, C.; Keyshar, K.; Zhang, X.; Yang, Y.; Ye, M.; Vajtai, R.; Lou, J.; Ajayan, P. M. Liquid Phase Exfoliation of Two-Dimensional Materials by Directly Probing and Matching Surface Tension Components. *Nano Lett.* **2015**, *15*, 5449−5454.

(62) Shen, J.; Wu, J.; Wang, M.; Dong, P.; Xu, J.; Li, X.; Zhang, X.; Yuan, J.; Wang, X.; Ye, M.; Vajtai, R.; Lou, J.; Ajayan, P. M. Surface Tension Components Based Selection of Cosolvents for Efficient Liquid Phase Exfoliation of 2D Materials. *Small* **2016**, *12*, 2741−2749.

(63) Yu, X.; Prévot, M. S.; Sivula, K. Multiflake Thin Film Electronic Devices of Solution Processed 2D MoS2 Enabled by Sonopolymer Assisted Exfoliation and Surface Modification. *Chem. Mater.* **2014**, *26*, 5892−5899.

(64) Luan, B.; Zhou, R. Wettability and friction of water on a MoS2 nanosheet. *Appl. Phys. Lett.* **2016**, *108*, 131601.

(65) Zhou, G.; Rajak, P.; Susarla, S.; Ajayan, P. M.; Kalia, R. K.; Nakano, A.; Vashishta, P. Molecular Simulation of MoS2 Exfoliation. *Sci. Rep.* **2018**, *8*, 16761.

(66) Tiberio, G.; Muccioli, L.; Berardi, R.; Zannoni, C. Towards in Silico Liquid Crystals. Realistic Transition Temperatures and Physical Properties for n-Cyanobiphenyls via Molecular Dynamics Simulations. *ChemPhysChem* **2009**, *10*, 125−136.

(67) Boyd, N. J.; Wilson, M. R. Optimization of the GAFF force field to describe liquid crystal molecules: the path to a dramatic improvement in transition temperature predictions. *Phys. Chem. Chem. Phys.* **2015**, *17*, 24851−24865.

(68) Boyd, N. J.; Wilson, M. R. Validating an optimized GAFF force field for liquid crystals: TNI predictions for bent-core mesogens and the first atomistic predictions of a dark conglomerate phase. *Phys. Chem. Chem. Phys.* **2018**, *20*, 1485−1496.

(69) Abraham, M. J.; Murtola, T.; Schulz, R.; Páll, S.; Smith, J. C.; Hess, B.; Lindahl, E. GROMACS: High performance molecular simulations through multi-level parallelism from laptops to supercomputers. *SoftwareX* **2015**, *1−2*, 19−25.

(70) Van Der Spoel, D.; Lindahl, E.; Hess, B.; Groenhof, G.; Mark, A. E.; Berendsen, H. J. C. GROMACS: Fast, flexible, and free. *J. Comput. Chem.* **2005**, *26*, 1701−1718.

(71) Essmann, U.; Perera, L.; Berkowitz, M. L.; Darden, T.; Lee, H.; Pedersen, L. G. A smooth particle mesh Ewald method. *J. Chem. Phys.* **1995**, *103*, 8577−8593.

(72) Bussi, G.; Donadio, D.; Parrinello, M. Canonical sampling through velocity rescaling. *J. Chem. Phys.* **2007**, *126*, 014101.

(73) Berendsen, H. J. C.; Postma, J. P. M.; Gunsteren, W. F. v.; DiNola, A.; Haak, J. R. Molecular dynamics with coupling to an external bath. *J. Chem. Phys.* **1984**, *81*, 3684−3690.

(74) Parrinello, M.; Rahman, A. Polymorphic transitions in single crystals: A new molecular dynamics method. *J. Appl. Phys.* **1981**, *52*, 7182−7190.

(75) Hess, B.; Bekker, H.; Berendsen, H. J. C.; Fraaije, J. G. E. M. LINCS: A linear constraint solver for molecular simulations. *J. Comput. Chem.* **1997**, *18*, 1463−1472.

(76) Gowers, R. J.; Linke, M.; Barnoud, J.; Reddy, T. J. E.; Melo, M. N.; Seyler, S. L.; Domanski, J.; Dotson, D. L.; Buchoux, S.; Kenney, I. M. *MDAnalysis: a Python package for the rapid analysis of molecular dynamics simulations*; Los Alamos National Lab (LANL): Los Alamos, NM, 2019; pp 2575−9752.

(77) Humphrey, W.; Dalke, A.; Schulten, K. VMD: Visual molecular dynamics. *J. Mol. Graphics* **1996**, *14*, 33−38.

(78) Momma, K.; Izumi, F. VESTA 3 for three-dimensional visualization of crystal, volumetric and morphology data. *J. Appl. Crystallogr.* **2011**, *44*, 1272−1276.